Inorganic Chemistry

pubs.acs.org/IC

Article

Comprehensive Investigation of [Fe(EDTA)]$^{-}$-Functionalized Derivatives and their Supramolecular Adducts with Human Serum Albumin

Alessandro Nucera, Maria Ludovica Macchia, Zsolt Baranyai,* Fabio Carniato, Lorenzo Tei, Mauro Ravera, and Mauro Botta*

Cite This: *Inorg. Chem.* 2024, 63, 12992−13004

Read Online

ACCESS | Metrics & More | Article Recommendations | Supporting Information

ABSTRACT: In recent years, the coordination chemistry of high-spin Fe(III) complexes has increasingly attracted interest due to their potential as effective alternatives to Gd(III)-based MRI contrast agents. This paper discusses the results from our study on Fe(III) complexes with two EDTA derivatives, each modified with either one (EDTA-BOM) or two (EDTA-BOM$_2$) benzyloxymethylene (BOM) groups on the acetic arm(s). These pendant hydrophobic groups enable the complexes to form noncovalent adducts with human serum albumin (HSA), leading to an observed increase in relaxivity due to the reduction in molecular tumbling. Our research involved detailed relaxometric measurements and analyses of both ^{1}H and ^{17}O NMR data at varying temperatures and magnetic field strengths, which is conducted with and without the presence of a protein. A significant finding of this study is the effect of electronic relaxation time on the effectiveness of [Fe(EDTA-BOM)(H$_2$O)]$^{-}$ and [Fe(EDTA-BOM$_2$)(H$_2$O)]$^{-}$ as diagnostic MRI probes. By integrating these relaxometric results with comprehensive thermodynamic, kinetic, and electrochemical data, we have thoroughly characterized how structural modifications to the EDTA base ligand influence the properties of the complexes.

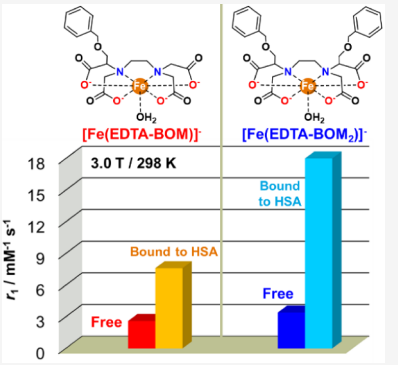

INTRODUCTION

The rapid development and widespread adoption of MRI as a clinical diagnostic modality have been facilitated by the parallel advancement of gadolinium-based contrast agents (GBCAs). These agents consist of small complexes with polyaminocarboxylic ligands, both acyclic and macrocyclic, wherein the Gd(III) ion exhibits high thermodynamic stability, good kinetic inertness, and the presence of a water molecule within its first coordination sphere that undergoes rapid exchange with the bulk.[1,2] Currently, nearly 50% of MRI examinations involve the administration of a GBCA. Despite the evident diagnostic benefits and their excellent safety profile, recent issues have spurred research into potential effective alternatives.[3,4] These issues include the incidence of nephrogenic systemic fibrosis linked to the administration of GBCAs in patients with severely impaired kidney function,[5] the deposition of trace amounts of Gd(III) in the tissues of patients who have received multiple doses of GBCAs,[6,7] and the increasing levels of anthropogenic gadolinium in surface water around densely populated areas.[8]

Low-molecular-weight iron(III) complexes are currently being investigated as a potential alternative to Gd(III) complexes used in MRI diagnostics.[9−17] They could address both concerns mentioned above, if their effectiveness as contrast agents proves to be comparable to that of GBCAs. From a coordination chemistry perspective, it is essential to find the optimal compromise among various requirements: high thermodynamic and redox stability, pronounced kinetic inertness, good ability to enhance the nuclear magnetic relaxation of water protons, and high solubility.[17]

Unlike Mn(II), monohydrated complexes of Fe(III) such as [Fe(EDTA)]$^{-}$ and [Fe(CDTA)]$^{-}$ exhibit high log K values and good stability over a wide range of pH values.[14] Their relaxometric properties have been recently investigated through a detailed analysis of ^{1}H NMRD and ^{17}O NMR data. A particularly notable result was the determination that the relaxivity (efficiency) at typical magnetic field strengths for imaging is controlled not only by rapid molecular tumbling (described by the rotational correlation time, τ_R) but also by the electronic relaxation time of the metal ion.[18]

This observation is crucial for developing complexes characterized by a high relaxivity (r_1). In the case of Gd(III) and Mn(II) complexes studied over the last two to three decades, r_1 is limited by τ_R, and larger values can be achieved

Received: April 26, 2024
Revised: June 10, 2024
Accepted: June 10, 2024
Published: July 1, 2024

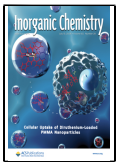

https://doi.org/10.1021/acs.inorgchem.4c01715
Inorg. Chem. 2024, 63, 12992−13004

by slowing down the rotational dynamics.[19] This can be accomplished by either increasing the molecular size of the complexes through appropriate chelate modifications[20] or promoting metal−complex interactions with macromolecular substrates.[21,22] A particularly effective strategy to achieve high relaxivity has proven to be the formation of host−guest noncovalent interactions between suitably functionalized complexes and slowly tumbling substrates. A major advantage is preservation of the structural integrity of the complex, allowing for easy excretion. Furthermore, the nature of the targeting group of the ligand dictates the strength of the interaction.

Making reasonable predictions about the behavior of Fe(III) complexes based on the reported data for analogous Gd(III) and Mn(II) complexes is currently impossible due to the influence of electronic relaxation on the r_1 values. In this study, we investigated Fe(III) complexes with derivatives of EDTA functionalized on the acetic arms with one (EDTA-BOM) or two (EDTA-BOM_2) benzyloxymethylene (BOM) groups (Scheme 1). The objective is to explore the effects of ligand

Scheme 1. Chemical Structure of the Ligands Discussed in the Text

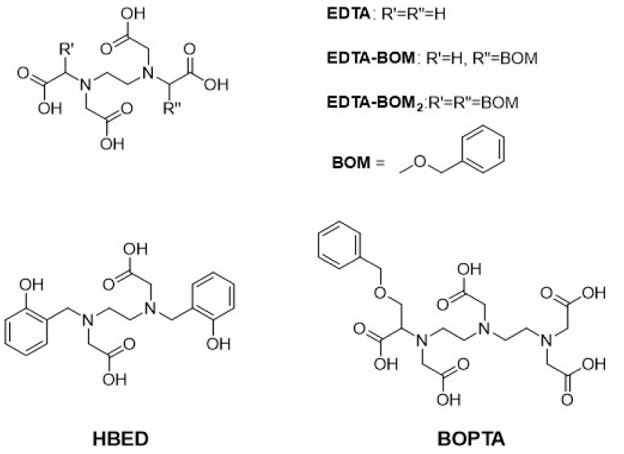

modification on thermodynamic, kinetic, and redox stability as well as relaxometric properties. Regarding the latter, the focus is particularly on verifying the possibility of modifying electronic relaxation through appropriate ligand modifications and assessing whether, in the case of Fe(III) complexes as well, the slowing down of molecular tumbling results in a significant relaxivity enhancement. Finally, in this case, there is a clear interest in understanding the characteristics of the relaxivity peak, in terms of amplitude and observation frequency, which is observed whenever the values of τ_R lengthen by approximately one or more orders of magnitude. We expect a shift of the maximum r_1 to higher frequency values due to the shorter electronic relaxation of Fe(III).

The choice of the BOM substituent is due to its well-known ability to promote noncovalent interactions with substrates, such as poly-β-cyclodextrins (poly-β-CD) and human serum albumin (HSA).[23−27] Therefore, we measured, for the two new complexes, the ^{1}H NMRD profiles at four different temperature values, transverse relaxation rates, and ^{17}O NMR shift data for thermodynamic stability constants, kinetic inertial characteristics, and redox properties. Furthermore, the noncovalent interaction of $[Fe(EDTA\text{-}BOM)(H_2O)]^-$ and $[Fe(EDTA\text{-}BOM_2)(H_2O)]^-$ with HSA was studied through relaxometric titrations at a fixed frequency (120 MHz) and by measuring NMRD profiles. The obtained results were compared with data related to the parent complex $[Fe(EDTA)(H_2O)]^-$ and those reported in the literature for corresponding Mn(II) complexes.[27]

EXPERIMENTAL SECTION

Materials. The chemicals used for the experiments were of the highest analytical grade. $Fe(NO_3)_3$ was prepared by dissolving Fe_2O_3 (99.9%, Fluka) in 6 M HNO_3 and evaporating the excess acid. The solid $Fe(NO_3)_3$ was dissolved in a 0.1 M HNO_3 solution. The concentration of the $Fe(NO_3)_3$ solution was determined by using standardized Na_2H_2EDTA in excess.[28] The excess of Na_2H_2EDTA was measured with standardized $ZnCl_2$ solution and xylenol orange as an indicator.[29] The H^+ concentration of the $Fe(NO_3)_3$ solution was determined by pH potentiometric titration in the presence of excess Na_2H_2EDTA. The concentrations of the H_4EDTA-BOM, H_4EDTA-BOM_2, and H_2HBED solution were determined by pH-potentiometric titrations in the presence and absence of a 40-fold excess of Ca^{2+}.[14] The pH-potentiometric titrations were performed with standardized 0.2 M NaOH.

Synthesis of the Ligands and Iron(III) Chelates. The ligands EDTA-BOM and EDTA-BOM_2 were synthesized according to literature procedures.[27] Briefly, the potassium salt of 3-benzyloxy-2-chloropropanoic acid was reacted with ethylenediamine (13 and 0.33 equiv with respect to the alkylating reagent, respectively) in H_2O, followed by exhaustive alkylation with 2-bromoacetic acid in a pH 10 water solution. $[Fe(EDTA\text{-}BOM)]^-$ and $[Fe(EDTA\text{-}BOM_2)]^-$ were synthesized by adding 1 equiv of the $Fe(NO_3)_3$ stock solution to the solution of the ligands (1.05 equiv) at pH = 2. After the addition, the pH was set to 2.5 with NaOH 0.1 M, and the samples were left under stirring for 2 h at room temperature. Then, the samples are brought to pH 7 with NaOH and left under stirring for 1 h. The samples were then filtered with a syringe. The complexes were checked through ESI-MS. $[Fe(EDTA\text{-}BOM)]^-$: MS (ESI$^+$): m/z calcd. for $C_{18}H_{20}FeN_2O_9$: 464.21; found: 466.45 ($M+2H^+$); $[Fe(EDTA\text{-}BOM_2)]^-$. MS (ESI$^+$): m/z calcd. for $C_{26}H_{28}FeN_2O_{10}$: 584.36; found: 586.66 ($M+2H^+$), 608.62 ($M+H^++Na^+$), 630.64 ($M+2Na^+$).

METHODS

Equilibrium Measurements. The stability and protonation constants of Fe(III) complexes formed with EDTA-BOM and EDTA-BOM_2 ligands were determined by pH-potentiometric and spectrophotometric studies. The protonation and dimerization constants of the $[Fe(EDTA\text{-}BOM)]^-$ and $[Fe(EDTA\text{-}BOM_2)]^-$ complexes were determined using pH-potentiometry by titrating the preprepared complexes from pH = 1.7 to pH = 12 with 0.2 M NaOH ([FeL] = 0.01 M). For the pH measurements and titrations, a *Metrohm 888 Titrando* titration workstation and a *Metrohm-6.0234.110* combined electrode were used. Equilibrium measurements were carried out at a constant ionic strength (0.15 M $NaNO_3$) and at 298 K in 6 mL solutions of the samples. The solutions were stirred, and N_2 was bubbled through them. The titrations were made in the pH range of 1.7−12.0. KH-phthalate (pH = 4.005), and borax (pH = 9.177) buffers were used to calibrate the pH meter. For the calculation of $[H^+]$ from the measured pH values, the method proposed by Irving was used.[30] Specifically,

https://doi.org/10.1021/acs.inorgchem.4c01715
Inorg. Chem. 2024, 63, 12992−13004

a 0.01 M HNO_3 solution was titrated with a standardized NaOH solution at 0.15 M $NaNO_3$ ionic strength. The differences (A) between the measured (pH_{read}) and calculated ($-\log[H^+]$) pH values were used to obtain the equilibrium H^+ concentration from the pH values measured in the titration experiments (A = 0.01). For equilibrium calculations, the stoichiometric ionic product of water (pK_w) must also be evaluated to calculate the $[OH^-]$ values under basic conditions. The V_{NaOH} − pH_{read} data pairs of the HNO_3−NaOH titration obtained in the pH range of 10.5−12.0 were used to calculate the pK_w value (pK_w = 13.81).

The protonation and dimerization processes of $[Fe(EDTA-BOM)]^-$ and $[Fe(EDTA-BOM_2)]^-$ were also investigated by spectrophotometric measurement in the wavelength range of 370−700 nm. Absorption spectra of the preprepared $[Fe(EDTA-BOM)]^-$ and $[Fe(EDTA-BOM_2)]^-$ complexes were recorded in the pH range 2.0−11.5 ([FeL] = 2.00 mM). The pH was adjusted by the stepwise addition of concentrated NaOH or HNO_3 solutions. All spectrophotometric measurements were performed at 298 K in a 0.15 M $NaNO_3$ solution. The spectrophotometric measurements were carried out using 1.0 cm cells on a *PerkinElmer Lambda 365* UV−vis spectrophotometer.

Capillary Electrophoresis. The stability constants of $[Fe(EDTA-BOM)]^-$ and $[Fe(EDTA-BOM_2)]^-$ were determined with capillary zone electrophoresis (CZE) by following the competition reaction in the Fe^{3+}-EDTA-BOM−EDTA and Fe^{3+}-EDTA-BOM_2−EDTA systems at pH = 4.0. Two series of eight samples were prepared with $[Fe^{3+}]$ = [EDTA-BOM] = 1.00 mM, $[Fe^{3+}]$ = $[EDTA-BOM_2]$ = 1.00 mM, and [EDTA] = 0.00, 0.26, 0.53, 0.99, 1.52, 1.98, 2.97, and 4.03 mM in 0.15 M $NaNO_3$ solution. The pH was adjusted to 4.0 by stepwise addition of concentrated NaOH and HNO_3 solutions. The samples were kept at 298 K for 2 weeks to ensure equilibrium is achieved (the time needed to reach the equilibria was determined by CZE). For the calculations of the stability constants of $[Fe(EDTA-BOM)]^-$ and $[Fe(EDTA-BOM_2)]^-$, the molar integral values of $[Fe(EDTA-BOM)]^-$, $[Fe(EDTA-BOM_2)]^-$, and $[Fe(EDTA)]^-$ were determined by recording the CZE electropherograms of 0.25, 0.50, 1.00, and 1.50 mM solutions of the Fe(III)-complexes. A *Hewlett-Packard HP^{3D}* capillary electrophoresis system was used for the CZE analyses. Separations were performed using bare fused-silica capillaries of 64 cm x 50 μm i.d. (*Agilent*). Before the first use, the capillary was washed with 1.0 M NaOH (15 min), 0.1 M NaOH (30 min), and the buffer electrolyte (30 min). Prior to CZE analysis, all buffers were filtered through a 0.45 μm syringe filter and stored in a refrigerator at 277 K. In CZE, the sample solutions were introduced at the anodic end of the capillary in normal mode (50 mbar, 2 s). The effective length of the capillary was 56 cm. The capillary was preconditioned with the buffer electrolyte (50 mM disodium hydrogen phosphate, pH = 6.0) for 3 min. The separation was performed at 298 K with the application of 25 kV voltage. After analysis, postconditioning (0.1 M NaOH) (3 min) and buffer washing (3 min) were run to remove all possible adsorbed materials from the capillary. In all measurements, 1 mM methyl orange as the internal standard was applied to correct the migration time of the components on the electropherogram. The detection was carried out by on-column DAD measurement at 190 nm. The electropherograms were recorded and processed by ChemStation B.04.02 version (*Agilent*). The individual linear regression equations (response−concentration) for all the Fe(III)-complexes were determined according to four concentrations. The peak areas were found to be linear ($R^2 \geq 0.998$) in a 0.25−1.50 mM concentration range of the complexes (precision better than 4%). The protonation and stability constants were calculated using the PSEQUAD program.[31]

Cyclic Voltammetry. Cyclic voltammetry measurements were carried out by using an *Autolab PGSTAT12 electrochemical analyzer* (Eco Chemie, Utrecht, The Netherlands) connected to a personal computer running GPES 4.9 electrochemical software. A standard three-electrode cell was constructed so that the tip of the reference electrode (Ag/AgCl, 3 M KCl) was close to the working electrode (a disk of glassy carbon (GC), diameter 0.1 cm, sealed in epoxy resin). The GC working electrode was polished with alumina, rinsed with distilled water, and dried. This procedure resulted in an almost completely reproducible surface for all of the experiments. Measurements were performed under nitrogen in Milli-Q water containing 0.15 M KNO_3 as a supporting electrolyte; the pH was set with nitric acid. The complex concentration was 1 mM. The temperature of the solution was kept constant (298 ± 1 K) by the circulation of a water/ethanol mixture through a jacketed cell. Positive feedback *iR* compensation was applied routinely. All peak potentials were measured at a scan rate of 0.2 V s^{-1} and reported vs the reference electrode.

Relaxometric Analysis. The ^1H $1/T_1$ NMRD profiles were obtained with a fast-field cycling Stelar SmartTracer relaxometer (Mede, Pavia, Italy) varying the magnetic-field strength from 0.00024 to 0.25 T (0.01−10 MHz range). The $1/T_1$ values were measured with an absolute uncertainty of ± 1%. Temperature was controlled with a Stelar VTC-91 airflow heater equipped with a calibrated copper−constantan thermocouple (uncertainty of ± 0.1 K). Data at high fields (0.5−3 T, corresponding to 20−128 MHz proton Larmor frequency) were collected with a high field relaxometer (Stelar) equipped with the HTS-110 3T metrology cryogen-free superconducting magnet. The measurements were performed with a standard inversion recovery sequence (20 experiments, 2 scans) with a typical 90° pulse width of 3.5 μs, and the reproducibility of the data was within ± 0.5%. The concentrations of the Fe(III) chelates were determined using ICP-MS. To validate these results, the chelates were mineralized in concentrated nitric acid at 80 °C overnight to produce the hexaaqua-ions. The longitudinal relaxation rate (R_1) of the acid solutions was measured at 60 MHz and 298 K, and the concentration was calculated based on the known relaxivity of the aqua-ion at the same field and temperature (r_1 = 12.9 mM^{-1} s^{-1}).[14] The agreement between the results obtained with the two methods is excellent.

^{17}O NMR Measurements. The spectra were acquired on a Bruker Avance III spectrometer (11.7 T) using a 5 mm probe under temperature control. An aqueous solution of the complexes was enriched to reach 2.0% of the ^{17}O isotope (Cambridge Isotope). The transverse relaxation rates were measured from the signal width at half-height as a function of temperature in the 278−350 K range. The simultaneous fit of ^1H NMRD profiles and ^{17}O NMR data was performed with the *Micromath Scientist* computer program (version 2.0, Salt Lake City, UT, USA).

Magnetic Moment Calculation. The effective magnetic moments of the Fe(III) chelates were determined using Evans' method.[32] This involved measuring the ^1H chemical shift of *t*-BuOH in a solution of the complex, which had a known

https://doi.org/10.1021/acs.inorgchem.4c01715
Inorg. Chem. 2024, 63, 12992−13004

concentration ascertained through ICP-MS analysis. The values of the measured magnetic moments are reported in Table S1.

RESULTS AND DISCUSSION

Synthesis. The ligands EDTA-BOM and EDTA-BOM$_2$ bearing one and two benzyloxymethylene groups, respectively, were synthesized accordingly to literature procedures.[27] The Fe(III) complexes were obtained by reacting an aqueous solution of the ligand and iron(III) nitrate at pH 2.5 and then precipitating and filtering unreacted Fe(III) at basic pH.

Thermodynamic Properties of [Fe(EDTA-BOM)]$^-$ and [Fe(EDTA-BOM$_2$)]$^-$ Complexes. The stability and protonation constants of the Fe(III)-complexes formed with EDTA-BOM and EDTA-BOM$_2$ were calculated using pH-potentiometric, spectrophotometric, and capillary electrophoretic data (Tables 1 and 2). The experimental details, definitions, and equations used for the evaluation of the equilibrium and kinetic data are summarized in the Supporting Information.

Table 1. Protonation Constants of EDTA-BOM, EDTA-BOM$_2$, and EDTA

	EDTA-BOM	EDTA-BOM$_2$	EDTA[a]	
I	0.15 M $NaNO_3$		0.15 M $NaNO_3$[a]	0.1 M KNO_3[b]
log K_1^H	9.18 (1)	8.91 (1)	9.40	10.22
log K_2^H	5.84 (2)	6.04 (1)	6.10	6.18
log K_3^H	2.81 (2)	2.85 (2)	2.72	2.70
log K_4^H	2.16 (2)	2.36 (2)	2.08	2.00
log K_5^H	1.15 (5)		1.23	
$\sum$ log K_i^H	**19.99 ($-$log K_5^H)**	**20.16**	**20.29 ($-$log K_5^H)**	**21.10**

[a]Reference 14. [b]Reference 33.

Upon comparing the literature data for EDTA-BOM and EDTA-BOM$_2$,[27] we observe that the first protonation constant is nearly an order of magnitude lower. This discrepancy can be attributed to the use of different salts to maintain constant ionic strength (KCl 0.1 M, 20 °C). Compared to EDTA, the log K_1^H value of EDTA-BOM and EDTA-BOM$_2$ decreases by about 0.22 and 0.49 log K unit, whereas the log K_{2-5}^H values are very similar. It is well-known that the first protonation of EDTA and its derivatives takes place on the N donor atom of the ligand backbone. The incorporation of the benzyloxymethylene unit(s) on the acetate pendant(s) can reduce the log K_1^H value of EDTA-BOM and EDTA-BOM$_2$ due to the electron withdrawal properties of the ether oxygen atom. A similar behavior is observed by comparing the log K_i^H values of the related ligands BOPTA and DTPA (BOPTA = 4-carboxy-5,8,11-tris(carboxymethyl)-1-phenyl-2-oxa-5,8,11-triazatridecan-13-oic acid, Scheme 1).[36]

On the other hand, the $\sum$log K_i^H values presented in Table 1 (25 °C; 0.15 M $NaNO_3$) show that the total basicity of EDTA-BOM, EDTA-BOM$_2$, and EDTA is very similar, suggesting that the stability constants of Fe(III) complexes with EDTA-BOM and EDTA-BOM$_2$ are fully comparable to that with EDTA. In fact, the stability constants of [Fe(EDTA)]$^-$ and [Fe(EDTA-BOM)]$^-$ (Table 2) are very similar and only slightly higher than that of [Fe(EDTA-BOM$_2$)]$^-$, which indicates a somehow weaker interaction of Fe(III) with EDTA-BOM$_2$. Conversely, the equilibrium constants characterizing deprotonation of the coordinated water molecule (logK_{FeLH-1}) are very similar for the three complexes. Another similarity between [Fe(EDTA-BOM)]$^-$ and [Fe(EDTA)]$^-$ can be found in the equilibrium constants characterizing the formation of oxo-bridged dimers (K_D and K_d; ESI), confirming that the introduction of one benzyloxymethylene group on an acetate pendant arm does not influence the equilibrium properties of the Fe(III) complexes. However, the solution properties of [Fe(EDTA-BOM$_2$)]$^-$ at pH > 6.0 differ considerably from those of [Fe(EDTA-BOM)]$^-$. In fact, the pH-potentiometric titration curve of [Fe(EDTA-BOM$_2$)]$^-$ shows two base consuming processes with well separated plateaus in the pH ranges 6.5−8.4 and 8.4−10.0. The best fitting was obtained by using the model, which includes the formation of the [FeL], [Fe(L)H$_{-1}$], [(FeL)$_2$H$_{-1}$], and [Fe(L)H$_{-2}$] species in equilibrium. These processes can be explained by the hydrolysis of the Fe(III) ion, accompanied by the coordination of one and two OH^- ions (eqs (S5) and (S8)), and by the dimerization of [FeL] via the formation of a μ−OH-bridged dimer (eq (S9)).

Using the equilibrium constants of Table 2, the species distributions of the Fe^{3+}-EDTA-BOM and Fe^{3+}-EDTA-BOM$_2$ systems were calculated as a function of pH (Figures 1,2). The species distribution of Fe^{3+}-EDTA-BOM is quite similar to that of Fe^{3+}-EDTA,[14] whereas the speciation of Fe^{3+}-EDTA-BOM$_2$ is considerably different at pH > 6.0.

Surprisingly, in this case, the oxo-bridged [(FeL)$_2$(μ−OH)] dimer has a very low abundance, possibly due to the favored formation of Fe(L)H$_{-2}$ species, which could occur through the substitution of the carboxylate O^- with an OH^- ion in [Fe(EDTA-BOM$_2$)H$_{-1}$]$^{2-}$. It is reasonable to assume that the weakly coordinated O^- of an acetate group functionalized with

Table 2. Stability Constants of Fe(III) and Mn(II)-Complexes with EDTA-BOM, EDTA-BOM$_2$, and EDTA Ligands (25°C)

	EDTA-BOM		EDTA-BOM$_2$		EDTA		
	Fe(III)	Mn(II)	Fe(III)	Mn(II)	Fe(III)		Mn(II)
I	0.15 M $NaNO_3$	0.1 M KCl[c]	0.15 M $NaNO_3$	0.1 M KCl[c]	0.15 M $NaNO_3$[a]	0.1 M KNO_3[b]	0.1 M KCl[d]
log K_{ML}	22.25 (5)	13.5	21.81 (7)	13.8	**22.14**	**24.95**	13.58
log K_{MHL}					1.12		
log K_{MLH-1}	7.56 (1)		7.59 (1)		7.51	7.52	
$-$log K_D	12.92 (4)				13.00	12.40	
log K_d	2.21 (3)				2.02	2.64	
log $\beta_{(ML)2H-1}$			−5.67 (5)				
log K_{MLH-2}			9.70 (1)				

[a]Reference 14. [b]Reference 34. [c]Reference 27 (0.1 M KCl, 20 °C). [d]Reference 35 (0.1 M KCl, 20 °C).

https://doi.org/10.1021/acs.inorgchem.4c01715
Inorg. Chem. 2024, 63, 12992−13004

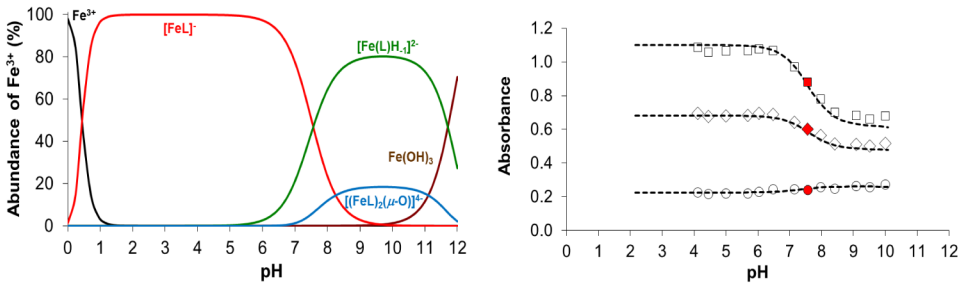

Figure 1. Species distribution (left) and absorbance values (right) of Fe^{3+}-EDTA-BOM system as a function of pH ([Fe^{3+}] = [EDTA-BOM] = 1.0 mM, λ = 395 (□), 410 (◊) and 470 nm (○), 25 °C, 0.15 M $NaNO_3$).

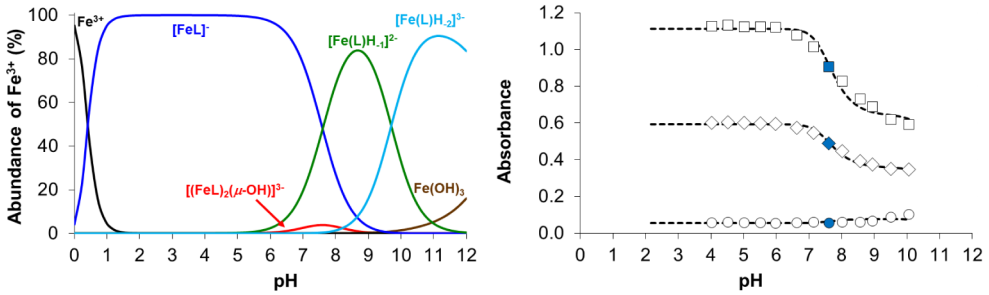

Figure 2. Species distribution (left) and absorbance values (right) of Fe^{3+}-EDTA-BOM_2 system as a function of pH ([Fe^{3+}] = [EDTA-BOM_2] = 1.0 mM, λ = 395 (□), 410 (◊) and 470 nm (○), 25 °C, 0.15 M $NaNO_3$).

a BOM unit is replaced by an OH^- in the formation of the $[Fe(EDTA\text{-}BOM_2)H_{-2}]^{3-}$.

Kinetic Inertness of [Fe(EDTA-BOM)]$^-$ and [Fe(EDTA-BOM$_2$)]$^-$ Complexes. The kinetic inertness of [Fe(EDTA-BOM)]$^-$ and [Fe(EDTA-BOM$_2$)]$^-$ complexes was determined by following their transchelation reactions with the ligand *N*,*N*′-bis(2-hydroxybenzyl) ethylenediamine-*N*,*N*′-diacetic acid (HBED) with spectrophotometry in the pH range 9.0−11.0 (Figure S3). [Fe(HBED)]$^-$ is characterized by a very high stability constant (log $K_{Fe(HBED)}$ = 39.68; 0.1 M KNO_3, 25 °C),[37] which allows to study the transchelation reactions even at very basic conditions (pH > 12).[14] The ligand exchange reactions were investigated in the presence of 10- and 20-fold excess of HBED to establish pseudo-first-order kinetic conditions ([FeL] = 0.2 mM, 0.15 M $NaNO_3$, 25 °C). The proposed mechanism for the transchelation of [Fe(EDTA-BOM)]$^-$ and [Fe(EDTA-BOM$_2$)]$^-$ is shown in Scheme 2, whereas the definitions and equations used for the evaluation of the kinetic data are reported in the ESI.

Scheme 2. Proposed Reaction Mechanism for the Transchelation Reactions of [Fe(EDTA-BOM)]$^-$ and [Fe(EDTA-BOM$_2$)]$^-$ with HBED

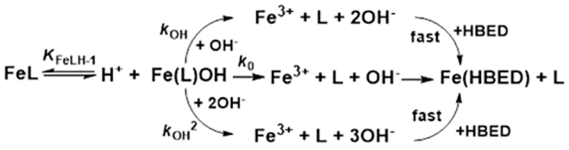

The reaction occurs via both spontaneous dissociation (k_0) and hydroxide-assisted dissociation of first and second order (k_1^{OH} and k_2^{OH}, respectively, Table 3) of the $Fe(L)H_{-1}$ species formed at pH > 6.0 (the formation of the dimeric $[(FeL)_2(\mu\text{-}O)]$ or $[(FeL)_2(\mu{-}OH)]$ species can be neglected in our experimental condition). The comparison of the rate constants

Table 3. Rate (k_i), Equilibrium Constants (K_{FeLH-1}), and Half-lives ($t_{1/2}$ = ln 2/k_d) Characterizing the Dissociation Reactions of [Fe(EDTA-BOM)]$^-$, [Fe(EDTA-BOM$_2$)]$^-$, and [Fe(EDTA)]$^-$ in the Absence and Presence of 0.6 mM HSA (0.15 M $NaNO_3$, 25°C)

	[Fe(EDTA-BOM)]$^-$	[Fe(EDTA-BOM$_2$)]$^-$	[Fe(EDTA)]$^-$[a]
$k_0/10^{-6}$ (s^{-1})	6 ± 1	14 ± 5	5
k_1^{OH} (M^{-1} s^{-1})	0.20 ± 0.03	0.50 ± 0.05	1.0
$k_2^{OH}/10^3$ (M^{-2} s^{-1})	1.0 ± 0.2	3.6 ± 0.4	1.4
log K_{FeLH-1}	7.56	7.59	7.41
$k_d/10^{-6}$at pH = 7.4 (s^{-1})	6.1	15	2.9
$t_{1/2}$at pH = 7.4(h)	31.6	13.2	66
$k_d/10^{-6}$ (s^{-1})[b]	2.8	3.4	
$t_{1/2}$(h)[b]	68	56	

[a]Reference 14. [b]At pH = 7.4, in the presence of 0.6 mM HSA.

reported in Table 3 indicates that the spontaneous dissociation of $Fe(L)H_{-1}$ species formed by [Fe(EDTA-BOM)]$^-$ and [Fe(EDTA)]$^-$ occurs at similar rates, approximately 2−3 times slower than that of [Fe(EDTA-BOM$_2$)]$^-$. The faster spontaneous dissociation of [Fe(EDTA-BOM$_2$)]$^-$ might be explained by a weaker interaction between Fe(III) and the O^- donor atom of the pendant arms carrying the BOM moieties, resulting in a faster intramolecular rearrangement of the $[Fe(EDTA\text{-}BOM_2)H_{-1}]^{2-}$ species. Considering that the dissociation rate constant (k_d) of both [Fe(EDTA-BOM)]$^-$ and [Fe(EDTA-BOM$_2$)]$^-$, calculated at pH = 7.4 and 25 °C, are about two and three times, respectively, higher than that of the parent [Fe(EDTA)]$^-$, it can be inferred that the latter Fe(III) complex is more inert.

It is widely recognized that the benzyloxymethylene unit of $[Gd(BOPTA)]^{2-}$ (Scheme 1; Multihance) is able to promote the formation of adducts with HSA through noncovalent hydrophobic interactions.[38] It is probable that the BOM units

https://doi.org/10.1021/acs.inorgchem.4c01715
Inorg. Chem. 2024, 63, 12992−13004

of the $[Fe(EDTA\text{-}BOM)]^-$ and $[Fe(EDTA\text{-}BOM_2)]^-$ complexes also facilitate interactions with HSA, potentially impacting their overall kinetic inertness related to the rate of Fe(III) release by the complexes. In fact, the dissociation rates of $[Fe(EDTA\text{-}BOM)]^-$ and $[Fe(EDTA\text{-}BOM_2)]^-$ near physiological conditions (0.15 M $NaNO_3$, 25 °C) are about 2 and 4 times slower in the presence of 0.6 mM HSA and very similar to that of $[Fe(EDTA)]^-$. It might be assumed that the "host–guest" adducts slow down the spontaneous release of Fe(III) from the chelates by reducing the flexibility of the complexes, as observed for $[Gd(BOPTA)]^{2-}$.[38]

Ascorbate Mediated Reduction of $[Fe(EDTA\text{-}BOM)]^-$ and $[Fe(EDTA\text{-}BOM_2)]^-$. A crucial property for *in vivo* applications of Fe(III) complexes is their redox stability. Fe(III)-based compounds can participate in the redox cycle by accepting electrons from reducing agents, leading to their reduction and the subsequent transfer of electrons to H_2O_2, which results in the formation of radicals (Fenton reaction).[39] According to the concentration[40] and the redox properties of the possible reducing agents in human blood plasma,[41,42] ascorbic acid is the most significant candidate likely to facilitate the involvement of Fe(III) complexes in the ascorbate-driven Fenton reaction. In our recent study, we underscored that ascorbic acid has the capability to reduce Fe(III) to Fe(II) in complexes involving EDTA and CDTA.[14] To monitor the reduction of the Fe(III) complexes of EDTA-BOM and EDTA-BOM_2 to their corresponding Fe(II) complexes, spectrophotometric measurements were conducted in the presence of a large excess of ascorbic acid, ensuring the establishment of pseudo-first-order kinetic conditions (Figure S4). The rate and equilibrium constants characterizing the reduction of $[Fe^{III}(EDTA\text{-}BOM)]^-$, $[Fe^{III}(EDTA\text{-}BOM_2)]^-$, and $[Fe^{III}(EDTA)]^-$ with ascorbic acid are reported in Table 4.

Table 4. Rate (k_i) and Equilibrium Constants ($K_{FeL\text{-}HA}$) and Half-lives ($t_{1/2} = \ln 2/k_d$) Characterizing the Ascorbic Acid Mediated Reduction of $[Fe(EDTA\text{-}BOM)]^-$, $[Fe(EDTA\text{-}BOM_2)]^-$ and $[Fe(EDTA)]^-$ (0.15 M $NaNO_3$, 25 °C)

	$[Fe(EDTA\text{-}BOM)]^-$	$[Fe(EDTA\text{-}BOM_2)]^-$	$[Fe(EDTA)]^-$[b]
k (M^{-1} s^{-1})[a]	20 ± 3	32 ± 5	8
$K_{FeL\text{-}HA}$(M^{-1})	71 ± 17	63 ± 19	75
log K_{FeLH-1}	7.56	7.59	7.51
$k_{obs}/10^{-4}$ (s^{-1})[c]	4.3	5.3	2.4
$t_{1/2}$(h)[c]	0.5	0.4	0.5

[a] $k = k_{HA}$ $K_{FeL\text{-}HA}$. [b] Reference 14. [c] Measured under physiological conditions.

According to the kinetic data, electron transfer occurs through the formation of a ternary {Fe(III)L–HA} intermediate between the ascorbate anion (HA^-) and the Fe(III)L complex, likely involving the substitution of the inner-sphere water molecule. The k rate constants characterizing the ascorbate anion assisted reduction of $[Fe(EDTA\text{-}BOM)]^-$ and $[Fe(EDTA\text{-}BOM_2)]^-$ are about 2 and 4 times higher than that of $[Fe(EDTA)]^-$ at pH = 7.4. On the other hand, the stability constant of the ternary {Fe(III)L–HA} intermediates ($K_{FeL\text{-}HA}$, Table 3) formed by $[Fe(EDTA\text{-}BOM)]^-$ and $[Fe(EDTA\text{-}BOM_2)]^-$ with ascorbate anion are very similar to that of $[Fe(EDTA)]^-$. By taking into account the K_{FeL-HA} values of these ternary intermediates and the *in vivo* concentration of the ascorbate anion ($[HA^-]$ = 43 μM),[40] the ascorbate assisted reduction rate (k_{obs}) and half-lives ($t_{1/2} = \ln 2/k_{obs}$) of $[Fe(EDTA\text{-}BOM)]^-$ and $[Fe(EDTA\text{-}BOM_2)]^-$ were found to be 4.3×10^{-4} and 5.3×10^{-4} s^{-1}, and 0.5 and 0.4 h, respectively. These $t_{1/2}$ values are more than 60 and 30 times greater than the dissociation half-lives of the Fe(III) complexes measured for the transchelation reactions with HBED, under identical condition (pH = 7.4, 25 °C, 0.15 M $NaNO_3$). This result implies that under similar conditions, the redox stability of $[Fe(EDTA\text{-}BOM)]^-$ and $[Fe(EDTA\text{-}BOM_2)]^-$ is significantly lower than their kinetic inertness.

Cyclic Voltammetry Studies of $[Fe(EDTA\text{-}BOM)]^-$, $[Fe(EDTA\text{-}BOM_2)]^-$, and $[Fe(EDTA)]^-$. In general, the rate constant for the oxidation of ascorbic acid assisted by an Fe(III) complex tends to decrease as the thermodynamic stability of the complex increases.[43–45] In this context, cyclic voltammetry was used to investigate the redox properties of $[Fe(EDTA\text{-}BOM)]^-$, $[Fe(EDTA\text{-}BOM_2)]^-$, and $[Fe(EDTA)]^-$. For these experiments, 1 mM water solutions of the complexes were prepared in 0.15 M KNO_3 as the supporting electrolyte, and the final pH was adjusted to 5.4. Examples of the cyclic voltammograms obtained by using a glassy carbon-working electrode are shown in Figure 3.

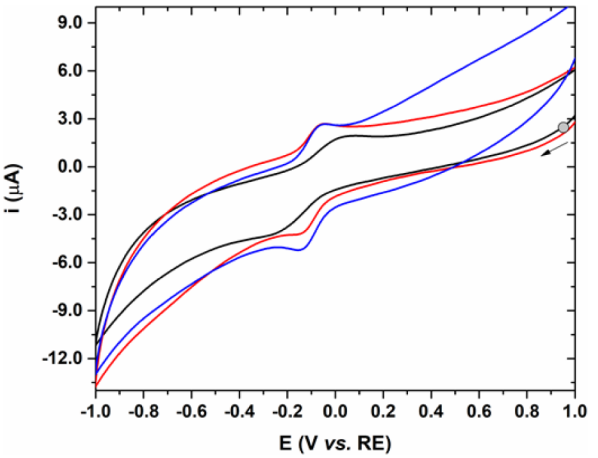

Figure 3. Cyclic voltammograms recorded for $[Fe(EDTA)]^-$ (black), $[Fe(EDTA\text{-}BOM)]^-$ (red), and $[Fe(EDTA\text{-}BOM_2)]^-$ (blue). Experimental conditions: 1 mM $[FeL]^-$ in an aqueous solution containing 0.15 M KNO_3 at pH = 5.4; working electrode = glassy carbon; scan rate = 0.2 V s^{-1}.

The half-wave potential ($E_{1/2}$) and peak-to-peak separation values (ΔE) obtained for $[Fe(EDTA\text{-}BOM)]^-$, $[Fe(EDTA\text{-}BOM_2)]^-$, and $[Fe(EDTA)]^-$ are listed in Table 5.

The cyclic voltammograms reported in Figure 3 show well-defined cathodic and anodic curves that indicate the presence of a chemically reversible Fe(III)/Fe(II) redox system. The $E_{1/2}$ obtained for the $[Fe(EDTA)]^-$ complex is in good agreement with that of the $E_{1/2}$ value reported in the

Table 5. Half-Wave Potentials ($E_{1/2}$, mV vs. Ag/AgCl, 3 M KCl at 0.2 V s^{-1}) and Peak-to-Peak Separations (ΔE, in the Scan Rate Range 0.05–3.0 V s^{-1}) for $[Fe(EDTA\text{-}BOM)]^-$, $[Fe(EDTA\text{-}BOM_2)]^-$, and $[Fe(EDTA)]^-$

	$[Fe(EDTA\text{-}BOM)]^-$	$[Fe(EDTA\text{-}BOM_2)]^-$	$[Fe(EDTA)]^-$
$E_{1/2}$ (mV)	−123 ± 5	−114 ± 6	−115 ± 8
ΔE (mV)	100–213	103–220	260–750

https://doi.org/10.1021/acs.inorgchem.4c01715
Inorg. Chem. 2024, 63, 12992–13004

literature.[16,34] As expected, the $E_{1/2}$ values of the three Fe(III) compounds are similar, being the same the coordination cage around the iron ion. More importantly, the higher peak-to-peak separation (ΔE) at every scan rate obtained for the $[Fe(EDTA)]^-$ system clearly indicates a slower Fe(III) → Fe(II) electron transfer process. This confirms the thermodynamically unfavorable structural rearrangement of the simple EDTA ligand with respect to the BOM derivatives to accommodate the Fe^{II} ion after the reduction step.

Relaxometry. In an aqueous solution, a complex containing a paramagnetic ion interacts with water molecules both within its inner coordination sphere (IS) and in the surrounding bulk (OS) through dipolar magnetic dipolar interactions. This coupling undergoes temporal modulation due to the exchange process of IS water molecules at a rate denoted as k_{ex} ($k_{ex} = 1/\tau_M$), the reorientation of the complex in solution (τ_R), and electronic relaxation ($T_{1,2e}$). Consequently, there is a significant augmentation in the nuclear magnetic relaxation rates of water protons (R_1 and R_2), which, when normalized to a 1 mM concentration of the paramagnetic ion, is termed relaxivity ($r_{1,2}$).[46,47] This parameter serves as a gauge for the efficacy of a paramagnetic complex as a relaxation agent. When assessing the potential of an Fe(III) complex as an MRI contrast agent, its relative effectiveness is assessed by measuring r_1 at one or more frequency values and then comparing these values with those of similar Gd(III) and Mn(II) complexes. r_1 represents the combined contributions from the inner sphere (IS) and outer sphere (OS) interactions ($r_1 = r_1^{IS} + r_1^{OS}$). Optimizing r_1 primarily focuses on the IS contribution as it depends on several parameters intricately linked to the molecular structure. This contribution scales with the number of coordinated water molecules (q) and is effectively described by the well-established Solomon–Bloembergen–Morgan (SBM) equations (eqs 1 and 2).[48−50]

$$r_1^{IS} = \frac{[Fe(III)]q}{55.56} \times \frac{1}{T_{1M} + \tau_M} \quad (1)$$

T_{1M} represents the relaxation time of the inner sphere water protons, influenced by factors such as their distance (r_{Fe-H}) from the metal ion, proton Larmor frequency, and correlation time τ_C, which characterizes the modulation of the magnetic dipolar coupling between nuclear and electronic spins (eq 2).

$$\frac{1}{\tau_{Ci}} = \frac{1}{\tau_R} + \frac{1}{\tau_M} + \frac{1}{T_{ie}} \quad i = 1, 2 \quad (2)$$

We anticipate that the two novel complexes, functionalized with one and two BOM moieties, respectively, maintain the fundamental structure of $[Fe(EDTA)(H_2O)]^-$ and thus the same hydration state. In such a scenario, the chemical alteration of the ligand should primarily affect the T_{1M} value, particularly the τ_R and T_{ie} parameters. The measured r_1 values at 60 MHz and 298 K (pH = 6) are 1.7, 2.2, and 2.9 mM^{-1} s^{-1} for $[Fe(EDTA)]^-$, $[Fe(EDTA\text{-}BOM)]^-$, and $[Fe(EDTA\text{-}BOM_2)]^-$, respectively. The notable increase in relaxivity correlates well with the increase in molecular mass resulting from the introduction of the substituents, which can be readily explained by a corresponding lengthening of the τ_R. These simple relaxivity values clearly indicate that all the three complexes are monohydrates ($q = 1$). The pH dependence of r_1 often provides useful information on speciation in solution, the stability range of the complexes, and the possible presence of hydrolysis phenomena. The data for the three complexes, measured at 120 MHz and 298 K, are shown in the figure (Figure 4).

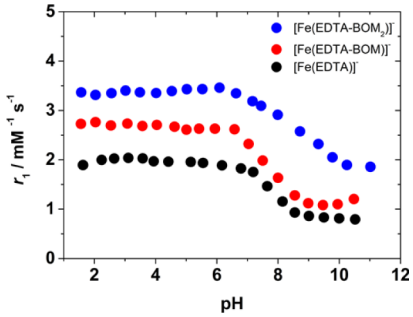

Figure 4. pH-dependency of r_1, at 120 MHz and 298 K, for $[Fe(EDTA\text{-}BOM_2)]^-$, $[Fe(EDTA\text{-}BOM)]^-$, and $[Fe(EDTA)]^-$.

The characteristic behavior of $[Fe(EDTA)]^-$ is closely mirrored in the two functionalized complexes. Within a broad pH range (pH = 2.5−6.5), r_1 remains relatively constant before sharply declining under basic conditions due to the deprotonation of the coordinated water molecule and subsequent formation of other complex species. The comprehensive relaxometric characterization was conducted at pH = 5.5 to ensure the stability of the complexes. Following a reliable and established protocol, the relaxometric analysis comprised measuring ^1H r_1 across various magnetic field strengths and temperatures, along with assessing the temperature dependence of the NMR transverse relaxation rate (R_2) and shift ($\Delta\omega$) of the ^{17}O nuclei of the water solvent.[51,52] The collection of relaxivity data across a broad spectrum of magnetic fields (ranging from 0.01 to 500 MHz) forms the $1/T_1$ NMRD (Nuclear Magnetic Relaxation Dispersion) profile. This profile undergoes a best-fit analysis using relevant equations for both IS and OS contributions, thereby deriving the molecular relaxation parameters. For both complexes the ^1H NMRD profiles were measured at four different temperatures, over the range 283−310 K (Figures S5 and S7). A comparison of the NMRD profiles of $[Fe(EDTA)]^-$, $[Fe(EDTA\text{-}BOM)]^-$, and $[Fe(EDTA\text{-}BOM_2)]^-$ obtained at 298 K is shown in Figure 5 (left). As shown in Figure 5 (left), the differences in r_1 values between the three complexes are smaller at high fields and more pronounced at low fields. This effect is due to the varying electronic relaxation times of the three complexes, which have a greater impact on relaxivity at low frequencies. In fact, the r_1 values of the three complexes exhibit a good linear correlation with their molecular masses only at high frequency (120 MHz; Figure S9). We also note that at every frequency the relaxivity of both complexes rises as temperature decreases, indicating they are in a fast exchange regime (where $\tau_M \ll T_{1M}$),[47] akin to the behavior of $[Fe(EDTA)]^-$. Hence, modification of the basic ligand seems to have minimal impact on the exchange process of the coordinated water molecule. This conclusion can be verified very accurately by the analysis of the ^{17}O NMR data collected at 11.7 T across various temperatures, as illustrated in Figure 5 (right) (see also Figures S6 and S8).[53] The reduction in transverse relaxation rates with decreasing temperature strongly corroborates the earlier findings. The simultaneous analysis of both ^1H and ^{17}O NMR relaxometric data yields essential relaxation parameters, with the most significant ones summarized in Table 6 (for the full list, refer to Table S2).

https://doi.org/10.1021/acs.inorgchem.4c01715
Inorg. Chem. 2024, 63, 12992−13004

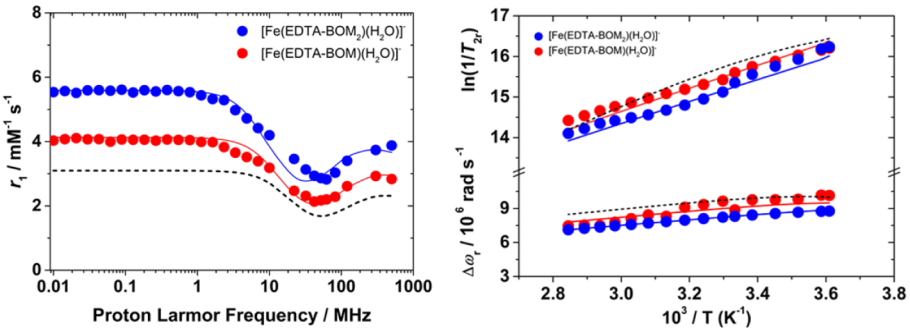

Figure 5. Left: ^{1}H NMRD profiles recorded at 298 K for $[Fe(EDTA\text{-}BOM_2)]^-$ and $[Fe(EDTA\text{-}BOM)]^-$. Right: reduced transverse relaxation rates and chemical shifts obtained for $[Fe(EDTA\text{-}BOM_2)]^-$ and $[Fe(EDTA\text{-}BOM)]^-$. In both cases, the solid lines represent the fits of the data, as described in the text. The dashed lines correspond to the curves of $[Fe(EDTA)]^-$ calculated with the data of ref 14.

Table 6. Parameters Obtained from the Simultaneous Fit of ^{1}H NMRD Profiles and ^{17}O NMR Data for the Fe(III) Complexes[a]

parameters	EDTA-BOM$_2$(MW = 584 g/mol)		EDTA-BOM (MW = 464 g/mol)		EDTA (MW = 344 g/mol)	
	Fe^{III}	Mn^{II} [b]	Fe^{III}	Mn^{II} [b]	Fe^{III} [c]	Mn^{II} [d]
$^{298}r_1$ 60 MHz/mM^{-1} s^{-1}	2.9	4.0	2.2	3.4	1.7	2.8
$^{298}\Delta^2/10^{20}$ s^{-2}	9.0 ± 0.5	0.53	19.1 ± 0.1	0.73	27.0	0.7
$^{298}\tau_V$/ps	3.9 ± 0.3	35.3	2.8 ± 0.3	24.7	2.8	27.7
$A_O/\hbar/10^6$ rad s^{-1}	−54.5 ± 0.6	37.9	−56.8 ± 0.5	37.9	−64.8[c]	40.5
$^{298}\tau_M{}^O$/ns	1.0 ± 0.1	7.6	1.0 ± 0.1	10.7	1	2.2
ΔH_M/ kJ mol^{-1}	23.0 ± 2.7	38.4	25.0 ± 2.5	43.1	30.5	33.5
$^{298}\tau_R$/ ps	78.0 ± 5.9	110.8	54.0 ± 6.7	83.7	35.1	56

[a]For comparison, the published parameters of the corresponding Mn(II) complexes are also reported. [b]Data from ref 27. [c]Data from ref 14. [d]Data from ref 54. q and r were fixed to 1 and 2.69 Å, respectively.

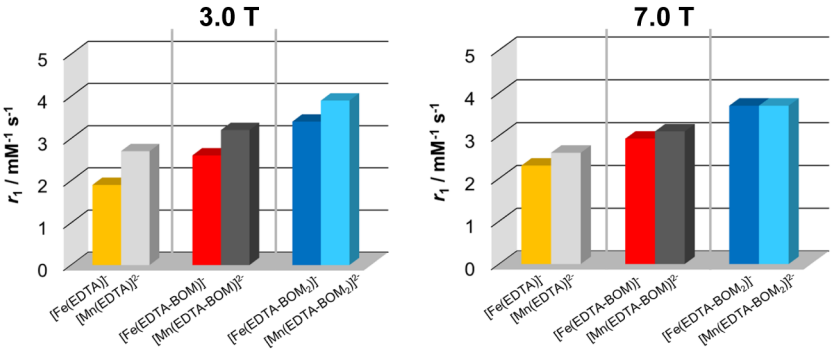

Figure 6. Comparison of r_1 values at 298 K measured at 3.0 (left) and 7.0 T (right) for the Fe^{III}- (yellow, red, and dark blue) and Mn^{II}-complexes (light gray, dark gray, and light blue) of EDTA, EDTA-BOM, and EDTA-BOM$_2$. The values for the Mn^{II} complexes are taken from refs 27 and 54.

The data clearly demonstrate a trend: passing from the parent complex to the mono- and disubstituted derivatives results in a deceleration of the rotational motion in solution, indicated by an increase in the correlation time (τ_R), consequently leading to higher relaxivity values (Figure S9). This observation aligns with previous findings in analogous Mn(II) complexes.[27] Notably, the exchange rate of the water molecule remains consistently high, unaffected by the introduction of substituents. However, the substituents exhibit a significant impact on the electronic relaxation time, evident from the significant decrease in the Δ^2 parameter by a third from $[Fe(EDTA)]^-$ to $[Fe(EDTA\text{-}BOM_2)]^-$.

It has been previously observed that, in contrast to Gd(III) and Mn(II) complexes, Fe(III) complexes exhibit shorter electronic relaxation times, contributing to the overall correlation time (τ_C) as per eq 2.[14] Consequently, since T_{1e} tends to increase with increasing magnetic field strength, relaxivity tends to increase at higher frequencies. This is evident when comparing the r_1 values for Fe(III) and Mn(II) complexes at 3 and 7 T and 298 K, as depicted in Figure 6. The difference in relaxivity between corresponding complexes diminishes at 7 T, which is particularly notable in the case of $[Fe(EDTA\text{-}BOM_2)]^-$, attributed to its lower Δ^2 value, indicative of a longer T_{1e}.

Interaction with HSA. The reversible formation of adducts with human serum albumin (HSA) has represented a prominent strategy for achieving greater relaxation enhancement in Gd(III) complexes, primarily attributed to the decreased rotational tumbling rate ($1/\tau_R$) within the macromolecular adduct.[55,56] Indeed, HSA has been extensively utilized for the noncovalent binding of Gd(III)/Mn(II) chelates featuring hydrophobic functionalities.[52] This approach

https://doi.org/10.1021/acs.inorgchem.4c01715
Inorg. Chem. 2024, 63, 12992−13004

capitalizes not only on the relaxivity enhancement induced by noncovalent interactions, but also on the prolonged circulation time of CA in the bloodstream.[57] The EDTA-BOM and EDTA-BOM_2 ligands feature hydrophobic pendant arms, endowing the respective Fe(III) complexes with the capacity to interact with HSA. This capability has been previously showcased in a study involving analogous Mn(II) complexes. Similarly, hydrophobic derivatives of $[Gd(DOTA)]^-$, employing similar pendant arms, have been developed to facilitate interaction with serum proteins.[25]

The properties of adducts formed by $[Fe(EDTA\text{-}BOM)]^-$ and $[Fe(EDTA\text{-}BOM_2)]^-$ with HSA were systematically investigated using the well-established ^1H proton relaxation enhancement (PRE) technique at pH 5.4, to ensure the stability of the complexes (Figures 1 and 2). This method involves measuring the variation in R_1 for increasing concentrations of the host protein.[58] According to the literature, HSA remains stable within the pH range of 5−7 without undergoing protein degradation or conformational changes.[59] The stability of HSA was also monitored by analyzing the ^1H NMRD profile of the protein (1.78 mM) across various pH values (from 5 to 8) at 298 K. The identical shape and amplitudes of the profiles confirm the high stability of albumin within the explored pH range (Figure S10). By titrating dilute solutions of $[Fe(EDTA\text{-}BOM)]^-$ and $[Fe(EDTA\text{-}BOM_2)]^-$ with HSA at 120 MHz and 298 K, a least-squares fit of the R_1 data versus HSA concentration binding isotherm (Figure 7) enabled the calculation of the affinity constant K_A and relaxivity of the resulting supramolecular adduct, r_1^b (Table 7). The fitting of experimental data was conducted assuming the presence of one equivalent and independent binding site (n = 1), although the existence of multiple, low-affinity sites on HSA cannot be discounted. The interaction between $[Fe(EDTA)]^-$ and HSA was also examined using the same procedure used for the other complexes. As expected, the results indicate that the complex does not exhibit any affinity for the protein (Figure 7).

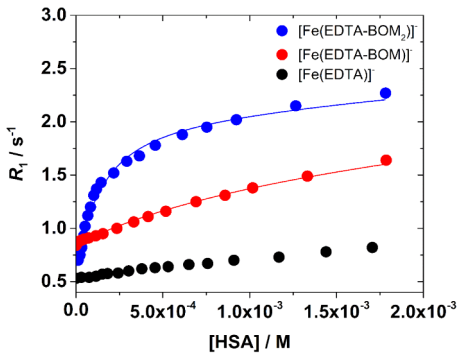

Figure 7. ^1H longitudinal relaxation rate of aqueous solutions of $[Fe(EDTA\text{-}BOM_2)]^-$, $[Fe^{3+}]$ = 0.094 mM), $[Fe(EDTA\text{-}BOM)]^-$, $[Fe^{3+}]$ = 0.18 mM), and $[Fe(EDTA)]^-$ ($[Fe^{3+}]$ = 0.079 mM) as a function of increasing amounts of HSA (120 MHz, 298 K, 50 mM MES buffer, pH = 5.4). The solid lines represent the fits of the data, as described in the text. The slight increase in R_1 with HSA concentration for $[Fe(EDTA)]^-$ is solely attributed to the protein's effect on the diamagnetic relaxation of water and does not suggest a binding interaction.

The strength of the binding interaction is influenced by both the charge of the complex and nature and number of hydrophobic substituents in the periphery of the chelator. The impact of charge is underscored by comparing the Fe(III) complexes investigated in this study with the corresponding Mn(II) complexes analyzed previously.[27] Notably, the association constant (K_A) for the Mn(II) complexes is approximately twice as large despite the molecular structures being identical. Given that the complexes $[Fe(EDTA\text{-}BOM)]^-$ and $[Fe(EDTA\text{-}BOM_2)]^-$ share the same coordination cage and binding moiety as the related Mn(II) complexes previously studied, we can reasonably assume that their interaction with HSA primarily involves the IIA subdomain of the protein.[27] Conversely, the Fe(III) complexes exhibit much stronger interactions with the protein compared to the corresponding derivatives $[Gd(DOTA\text{-}BOM)]^-$ and *cis*-$[Gd(DOTA\text{-}BOM)_2]^-$.[25] While this result lacks a straightforward explanation, it is likely attributable to differences in molecular structures and, consequently, varying degrees of steric interaction within the binding site.

Finally, the titration of $[Fe(EDTA\text{-}BOM_2)]^-$ with HSA was carried out also at pH 6 in MES buffer (2-morpholinoethanesulfonic acid) at 120 MHz and 298 K. The relaxometric titration and the related calculated binding data fully correspond to those obtained at pH = 5.4 (Figure S11). The combination of these results strongly suggests that a comparison between the complexes of Fe(III), Mn(II), and Gd(III) is both possible and reasonable, despite the differing pH values required to maintain the integrity of the Fe complex in solution.

At an identical chelate-to-protein molar ratio of 1:10, approximately 60% of $[Fe(EDTA\text{-}BOM)]^-$ and 89% of $[Fe(EDTA\text{-}BOM_2)]^-$ are bound to the protein. We conducted measurements of the NMRD profiles at 298 K, as depicted in the figure presented in terms of bound relaxivity, r_1^b (Figure 8). The r_1^b values were calculated using known values of r_1 for the free complexes and their association constants, K_A. For $[Fe(EDTA\text{-}BOM)]^-$, the NMRD profile of the HSA adduct displays a relatively broad and less intense peak, centered on approximately 100−120 MHz (Figure 8, left). At 120 MHz, the value of r_1^b is 120% greater than that of the free complex. The modest increase in r_1 could potentially be attributed to a high degree of rotational flexibility of the complex at the

Table 7. Binding Parameters and Relaxivity of the Adducts with HSA of the Fe(III) Complexes and Related Mn(II) and Gd(III) Chelates

Parameters	EDTA-BOM		EDTA-BOM_2		DOTA-BOM	DOTA-BOM_2
	Fe(III)	Mn(II)[a]	Fe(III)	Mn(II)[a]	Gd(III)[b]	
K_A M^{-1}	870±20	1500	9300±110	19000	<100	320
n	1[c]	1[c]	1[c]	1[c]	-	2[c]
r_1^b mM^{-1} s^{-1}	7.6±0.2	55.3	18.0±0.4	48.0	-	35.7

[a]Data from ref 27. [b]Data from ref 25. [c]Fixed during the analysis.

https://doi.org/10.1021/acs.inorgchem.4c01715
Inorg. Chem. 2024, 63, 12992−13004

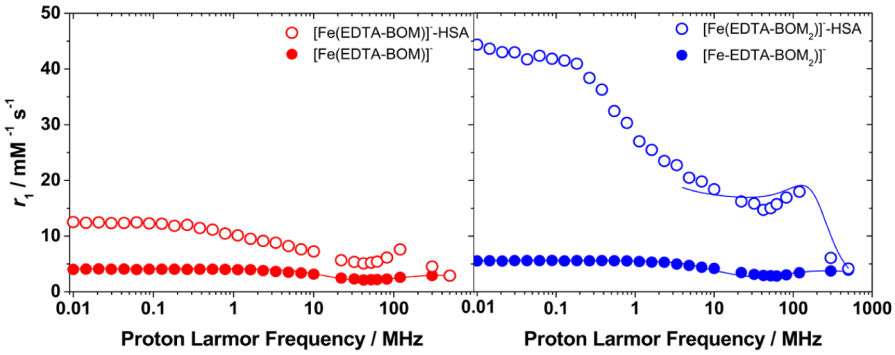

Figure 8. ^{1}H NMRD profiles (298 K) for: left, $[Fe(EDTA\text{-}BOM)]^{-}$ free and bound to HSA; right: $[Fe(EDTA\text{-}BOM_2)]^{-}$ free and bound to HSA. The solid lines represent fits of the data.

binding site, particularly around the BOM moiety, resulting in a shorter local rotational correlation time.

Conversely, $[Fe(EDTA\text{-}BOM_2)]^{-}$ features two targeting moieties, suggesting that if both engage in the binding interaction, the resulting bound complex should exhibit increased coupling between global and local motion. Indeed, the NMRD profile of the protein adduct in this scenario demonstrates a significantly higher amplitude and a more pronounced and well-defined peak with the maximum still centered at around 120 MHz. Due to the notable disparity in the relaxivity between the free and protein-bound complexes, our analysis focused solely on the disubstituted complex. Following a standard approach, we concentrated on data from the high-field region due to the recognized limitations of the SBM theory in accurately describing the behavior of slowly rotating systems at lower magnetic field strengths.[60] According to a well-established procedure, the rotational dynamics was described by the Lipari−Szabo model that takes into account the anisotropy of the motion of the bound complex, describable in terms of global tumbling and localized motions.[60] The global rotational correlation time was fixed to 50 ns in agreement to fluorescence data reported in the literature.[61] Nonetheless, it is worth noting that this value is somewhat arbitrary, as the fit outcomes remain unaffected by variations of this parameter within the range of about 20−1000 ns. During the data analysis, we initially set the water exchange rate to the value found for the free complex. However, this resulted in an unsatisfactory fit. When we allowed this parameter to vary, the quality of the fit improved significantly, despite the large associated uncertainty in τ_M. This might suggest that the bound water's lifetime is likely too short, impacting the overall correlation time. The best-fit parameters (Table 8) reveal that the adduct displays a modest correlation between global and local rotational motions, as evidenced by the considerable discrepancy between the local (τ_{RL}) and global (τ_{RG}) rotational correlation times. However, a more constrained molecular motion at the protein binding site may not guarantee a substantial further enhancement in relaxivity due to the limits imposed by the short electronic relaxation time. These shorter T_{1e} values diminish the value of τ_C (as per eq 2), somewhat offsetting the advantages gained from reduced molecular tumbling (resulting in longer τ_R).

Recently, we emphasized that even in low molecular weight Fe(III) complexes, T_{1e} contributes significantly to relaxivity.[14] As the mobility of the complex is substantially reduced and τ_R is consequently prolonged, the contribution of T_{1e} to the relaxivity further intensifies. This results in two effects: a decrease in the maximum value of r_1 and its shift toward higher magnetic fields compared to what is typically observed in systems based on Gd(III) and Mn(II). This is clearly demonstrated in the graph below (Figure 9), contrasting the

Table 8. Selected Best Fit Parameters of the ^{1}H NMRD Profile of $[Fe(EDTA\text{-}BOM_2)]^{-}$ Bound to HSA at 298 K[a]

Parameters	$[Fe(EDTA\text{-}BOM_2)]^{-}$	
	free	HSA-bound
$^{298}\Delta^2/10^{20}$ s^{-2}	9.0 ± 0.5	4.1 ± 0.2
$^{298}\tau_V$ (ps)	3.9 ± 0.3	0.8 ± 0.1
$^{298}\tau_M$ (ns)	1.0 ± 0.1	3.0 ± 1.0
$^{298}\tau_{RL}$ (ps)	-	779 ± 40
$^{298}\tau_{RG}$ (ns)	0.078 ± 0.0059	50 [a]
S^2	-	0.74 ± 0.05

[a]Fixed parameters.

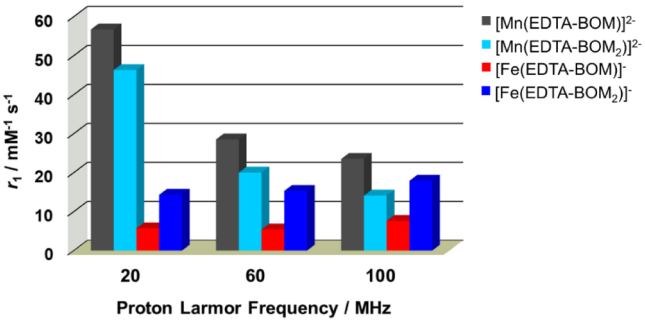

Figure 9. Comparison of r_1 values at 20, 60, and 100 MHz (298 K) for the adducts with HSA of $[Mn(EDTA\text{-}BOM)]^{2-}$,[26] $[Mn(EDTA\text{-}BOM_2)]^{2-}$,[26] $[Fe(EDTA\text{-}BOM)]^{-}$, and $[Fe(EDTA\text{-}BOM_2)]^{-}$.

$r_1{}^{b}$ values for the protein-bound complexes of Mn(II) and Fe(III) with those of EDTA-BOM and EDTA-BOM_2. At 20 and 60 MHz, it is evident that the Mn(II) complexes exhibit significantly greater effectiveness than their corresponding Fe(III) counterparts. However, at 100 MHz, the $r_1{}^{b}$ values of the two types of magnetic probes became much more comparable. Furthermore, at magnetic field strengths of 3T or higher, the effectiveness of Fe-based systems surpasses that of Mn-based systems (Figure 9).

However, these observations are primarily qualitative due to the absence of a robust electronic relaxation model for macromolecular systems. Indeed, it is worth pointing out that even for slowly tumbling complexes of both Mn(II) and

https://doi.org/10.1021/acs.inorgchem.4c01715
Inorg. Chem. 2024, 63, 12992−13004

Gd(III), the limitations of SBM theory in handling electronic relaxation have been frequently underscored.[62] Consequently, when the primary focus is on evaluating the rotational dynamics, only data at intermediate to high frequencies (>ca. 6 MHz) are often analyzed using SBM equations, treating electronic relaxation parameters as adjustable fitting parameters without assigning them specific physical interpretations.[63] In the case of Fe(III)-based systems, this consideration becomes even more crucial due to their faster electronic relaxation. This high relaxation rate significantly influences the relaxivity at high fields and consequently reduces the accuracy of the data analysis. The fitting outcomes exhibit minimal sensitivity to the value of τ_V, whereas they demonstrate considerable dependence on Δ^2, τ_{RL}, and S^2 (and τ_M). Considering these constraints, it is advisible to regard the calculated parameters merely as a rough approximation. Nonetheless, the obtained values of τ_{RL} and S^2 appear quite reasonable, based on our experience, and despite being subject to a large error, the value of τ_M closely resembles that of the free complex, as you would expect.

CONCLUSIONS

The strategy of leveraging noncovalent interactions between complexes functionalized with hydrophobic residues and macromolecular systems proves to be effective even for Fe(III) complexes. The nature of the hydrophobic substituent and the overall charge of the complex play similar roles in determining the strength of the interaction. However, certain characteristics of Fe(III) complexes set them apart from the well-established systems based on Gd(III) and Mn(II). Unlike Mn(II), the high thermodynamic stability of Fe(III) complexes renders the release of Fe^{3+} ions following the binding interaction with HSA highly improbable. Moreover, the very high coordinated water exchange rate, at least in $[Fe(EDTA)]^-$ and derivatives, implies that τ_M does not represent a limiting factor in the relaxivity of the protein-bound complex, unlike what has often been observed in Gd(III)-based systems. Furthermore, and perhaps more importantly, the role of T_{1e} is notably distinct in Fe(III)-based systems. With T_{1e} being considerably shorter compared to Mn(II) and Gd(III) complexes, it contributes to τ_C not only at low frequencies (approximately <10 MHz), but also at 100 MHz and beyond. This contribution becomes increasingly significant as molecular motion slows and τ_R lengthens. Figure 10 illustrates a simulation of the relaxivity values at 3 T as a function of τ_R and T_{1e}, emphasizing the pivotal role of electronic relaxation. It is important to acknowledge that while this simulation provides valuable insights, its rigor may be limited as it relies on the SBM model of paramagnetic relaxation, which may not be fully appropriate for slowly tumbling systems. Nonetheless, it clearly demonstrates that optimizing the efficacy of Fe-based MRI contrast agents hinges significantly more on lengthening T_{1e} than on slowing down rotation.

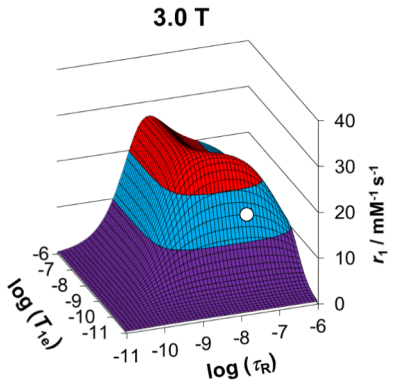

Figure 10. 3D plot representing r_1 of a slowly tumbling Fe(III)-complex as a function of the rotational correlation time (τ_R) and of the longitudinal electronic relaxation time (T_{1e}) at 3.0 T and 298 K. Other parameters are q = 1, r_{Fe-H} = 2.69 Å, and τ_M = 3.0 ns. The white circle (○) represents the experimental relaxivity value (r_1 = 18.0 mM^{-1} s^{-1}) calculated for the HSA adduct $[Fe(EDTA\text{-}BOM_2)]^-$ at the same magnetic field strength and temperature.

Then, an important objective of future studies will be to establish an empirical correlation between the structure of the complexes and the electronic relaxation parameters, thereby providing guidelines for the design of more efficient systems.

ASSOCIATED CONTENT

Supporting Information

The Supporting Information is available free of charge at https://pubs.acs.org/doi/10.1021/acs.inorgchem.4c01715.

Details on the thermodynamic and kinetic studies and redox stability of $[Fe(EDTA\text{-}BOM)]^-$ and $[Fe(EDTA\text{-}BOM_2)]^-$, ^{1}H NMRD and ^{17}O NMR data at different temperatures for $[Fe(EDTA\text{-}BOM)]^-$ and $[Fe(EDTA\text{-}BOM_2)]^-$, and r_1 values as a function of the molecular mass of different monohydrated Fe(III) chelates (PDF)

AUTHOR INFORMATION

Corresponding Authors

Zsolt Baranyai − *Bracco Imaging SpA, CRB Trieste, AREA Science Park, Basovizza, TS 34149, Italy;* orcid.org/0000-0001-6844-7974; Email: zsolt.baranyai@bracco.com

Mauro Botta − *Dipartimento di Scienze e Innovazione Tecnologica, Università del Piemonte Orientale, Alessandria 15121, Italy; Magnetic Resonance Platform (PRISMA-UPO), Università del Piemonte Orientale, Alessandria 15121, Italy;* orcid.org/0000-0003-4192-355X; Email: mauro.botta@uniupo.it

Authors

Alessandro Nucera − *Dipartimento di Scienze e Innovazione Tecnologica, Università del Piemonte Orientale, Alessandria 15121, Italy;* orcid.org/0000-0001-8916-4148

Maria Ludovica Macchia − *Dipartimento di Scienze e Innovazione Tecnologica, Università del Piemonte Orientale, Alessandria 15121, Italy;* orcid.org/0009-0001-8986-5718

Fabio Carniato − *Dipartimento di Scienze e Innovazione Tecnologica, Università del Piemonte Orientale, Alessandria 15121, Italy; Magnetic Resonance Platform (PRISMA-UPO), Università del Piemonte Orientale, Alessandria 15121, Italy;* orcid.org/0000-0002-6268-1687

Lorenzo Tei − *Dipartimento di Scienze e Innovazione Tecnologica, Università del Piemonte Orientale, Alessandria 15121, Italy;* orcid.org/0000-0002-7027-8396

Mauro Ravera − *Dipartimento di Scienze e Innovazione Tecnologica, Università del Piemonte Orientale, Alessandria 15121, Italy;* orcid.org/0000-0002-4732-7508

Complete contact information is available at: https://pubs.acs.org/10.1021/acs.inorgchem.4c01715

https://doi.org/10.1021/acs.inorgchem.4c01715
Inorg. Chem. 2024, 63, 12992−13004

Author Contributions

The manuscript was written through contributions of all authors. All authors have given approval to the final version of the manuscript.

Funding

Ministero dell'Università e della Ricerca: a) Project NODES which has received funding from the MUR−M4C2 1.5 of PNRR with grant agreement no.ECS00000036; b) PRIN 2022 PNRR (PNRR M4C2, ID P20224R8YZ). Hungarian National Research, Development, and Innovation Office (NKFIH K-21−139140 project)

Notes

The authors declare no competing financial interest.

■ ACKNOWLEDGMENTS

This publication is part of the project NODES, which has received funding (A.N., M.B.) from the Ministero dell'Università e della Ricerca (MUR−M4C2 1.5 of PNRR with grant agreement no. ECS00000036). F.C. acknowledges the Ministero dell'Università e della Ricerca (PRIN 2022, PNRR M4C2, ID P20224R8YZ). Z.B. thanks the financial support from the Hungarian National Research, Development, and Innovation Office (NKFIH K-21-139140 project).

■ REFERENCES

(1) Merbach, A. E.; Helm, L.; Toth, E. *The Chemistry of Contrast Agents in Medical Magnetic Resonance Imaging*, edn ed.; John Wiley & Sons Ltd, 2013.

(2) Wahsner, J.; Gale, E. M.; Rodríguez-Rodríguez, A.; Caravan, P. Chemistry of MRI Contrast Agents: Current Challenges and New Frontiers. *Chem. Rev.* **2019**, *119*, 957−1057.

(3) Caravan, P. Divalent Manganese Complexes as Potential Replacements for Gadolinium-Based Contrast Agents. *Invest. Radiol.* **2024**, *59* (2), 187−196.

(4) Botta, M.; Carniato, F.; Esteban-Gomez, D.; Platas-Iglesias, C.; Tei, L. Mn(II) compounds as an alternative to Gd-based MRI probes. *Future Med. Chem.* **2019**, *11*, 1461−1483.

(5) Hazelton, J. M.; Chiu, M. K.; Abujudeh, H. H. Nephrogenic Systemic Fibrosis: A Review of History, Pathophysiology, and Current Guidelines. *Curr. Radiol. Rep.* **2019**, *7*, 1−9.

(6) Gianolio, E.; Di Gregorio, E.; Aime, S. Chemical Insights into the Issues of Gd Retention in the Brain and Other Tissues Upon the Administration of Gd-Containing MRI Contrast Agents. *Eur. J. Inorg. Chem.* **2019**, *2019*, 137−151.

(7) Le Fur, M.; Caravan, P. The biological fate of gadolinium-based MRI contrast agents: a call to action for bioinorganic chemists. *Metallomics* **2019**, *11*, 240−254.

(8) Schmidt, K.; Bau, M.; Merschel, G.; Tepe, N. Anthropogenic gadolinium in tap water and in tap water-based beverages from fast-food franchises in six major cities in Germany. *Sci. Total Environ.* **2019**, *687*, 1401−1408.

(9) Lauffer, R. B.; Vincent, A. C.; Padmanabhan, S.; Villringer, A.; Saini, S.; Elmaleh, D. R.; Brady, T. J. Iron-EHPG as an hepatobiliary MR contrast agent: initial imaging and biodistribution studies. *Magn. Reson. Med.* **1987**, *4*, 582−590.

(10) Boehm-Sturm, P.; Haeckel, A.; Hauptmann, R.; Mueller, S.; Kuhl, C. K.; Schellenberger, E. A. Low-Molecular-Weight Iron Chelates May Be an Alternative to Gadolinium-based Contrast Agents for T_1-weighted Contrast-enhanced MR Imaging. *Radiology* **2018**, *286*, 537−546.

(11) Snyder, E. M.; Asik, D.; Abozeid, S. M.; Burgio, A.; Bateman, G.; Turowski, S. G.; Spernyak, J. A.; Morrow, J. R. A Class of Fe^{III} Macrocyclic Complexes with Alcohol Donor Groups as Effective T_1 MRI Contrast Agents. *Angew. Chem., Int. Ed.* **2020**, *59*, 2414−2419.

(12) Cineus, R.; Abozeid, S. M.; Sokolow, G. E.; Spernyak, J. A.; Morrow, J. R. Fe(III) T_1 MRI Probes Containing Phenolate or Hydroxypyridine-Appended Triamine Chelates and a Coordination Site for Bound Water. *Inorg. Chem.* **2023**, *62* (40), 16513−16522.

(13) Kras, E. A.; Cineus, R.; Crawley, M. R.; Morrow, J. R. Macrocyclic complexes of Fe(III) with mixed hydroxypropyl and phenolate or amide pendants as T_1 MRI probes. *Dalton Trans.* **2024**, *53*, 4154−4164.

(14) Baranyai, Z.; Carniato, F.; Nucera, A.; Horváth, D.; Tei, L.; Platas-Iglesias, C.; Botta, M. Defining the conditions for the development of the emerging class of Fe^{III}-based MRI contrast agents. *Chem. Sci.* **2021**, *12*, 11138−11145.

(15) Kuźnik, N.; Wyskocka, M.; Jarosz, M.; Oczek, L.; Goraus, S.; Komor, R.; Krawczyk, T.; Kempka, M. Amino-phenol complexes of Fe(III) as promising T_1 accelerators. *Arabian J. Chem.* **2019**, *12*, 1424−1435.

(16) Uzal-Varela, R.; Lucio-Martínez, F.; Nucera, A.; Botta, M.; Esteban-Gómez, D.; Valencia, L.; Rodríguez-Rodríguez, A.; Platas-Iglesias, C. A systematic investigation of the NMR relaxation properties of Fe(III)-EDTA derivatives and their potential as MRI contrast agents. *Inorg. Chem. Front.* **2023**, *10*, 1633−1649.

(17) Kras, E. A.; Snyder, E. M.; Sokolow, G. E.; Morrow, J. R. Distinct Coordination Chemistry of Fe(III)-Based MRI Probes. *Acc. Chem. Res.* **2022**, *55* (10), 1435−1444.

(18) *Contrast Agents for MRI: Experimental Methods*, Pierre, V. C.; Allen, M. J.; The Royal Society of Chemistry: Pierre, V.C, 2018.

(19) Botta, M.; Tei, L. Relaxivity Enhancement in Macromolecular and Nanosized Gd^{III}-Based MRI Contrast Agents. *Eur. J. Inorg. Chem.* **2012**, *2012*, 1945−1960.

(20) Maier, K. B.; Rust, L. N.; Carniato, F.; Botta, M.; Woods, M. α-Aryl substituted GdDOTA derivatives, the perfect contrast agents for MRI. *Chem. Commun.* **2024**, *60*, 2898−2901.

(21) Caravan, P. Protein-targeted gadolinium-based magnetic resonance imaging (MRI) contrast agents: design and mechanism of action. *Acc. Chem. Res.* **2009**, *42* (7), 851−862.

(22) Rolla, G. A.; De Biasio, V.; Giovenzana, G. B.; Botta, M.; Tei, L. Supramolecular assemblies based on amphiphilic Mn^{II}-complexes as high relaxivity MRI probes. *Dalton Trans.* **2018**, *47* (31), 10660−10670.

(23) Aime, S.; Botta, M.; Ermondi, G.; Fedeli, F.; Uggeri, F. Synthesis and NMRD Studies of Gd^{3+} Complexes of Macrocyclic Polyamino Polycarboxylic Ligands Bearing β-Benzyloxy-α-propionic Residues. *Inorg. Chem.* **1992**, *31*, 1100−1103.

(24) Aime, S.; Botta, M.; Panero, M.; Grandi, M.; Uggeri, F. Inclusion complexes between β-cyclodextrin and β-benzyloxy-α-propionic derivatives of paramagnetic DOTA- and DPTA-Gd(III) complexes. *Magn. Reson. Chem.* **1991**, *29*, 923−927.

(25) Aime, S.; Botta, M.; Fasano, M.; Crich, S. G.; Terreno, E. Gd(III) complexes as contrast agents for magnetic resonance imaging: a proton relaxation enhancement study of the interaction with human serum albumin. *J. Biol. Inorg. Chem.* **1996**, *1*, 312−319.

(26) Aime, S.; Chiaussa, M.; Digilio, G.; Gianolio, E.; Terreno, E. Contrast agents for magnetic resonance angiographic applications: ^1H and ^{17}O NMR relaxometric investigations on two gadolinium(III) DTPA-like chelates endowed with high binding affinity to human serum albumin. *J. Biol. Inorg. Chem.* **1999**, *4*, 766−774.

(27) Aime, S.; Anelli, P.; Botta, M.; Brocchetta, M.; Canton, S.; Fedeli, F.; Gianolio, E.; Terreno, E. Relaxometric evaluation of novel manganese(II) complexes for application as contrast agents in magnetic resonance imaging. *J. Biol. Inorg. Chem.* **2002**, *7*, 58−67.

(28) Schwarzenbach, G.*Flaschka, H.A, in Complexometric Titrations*, 2nd. Ed.; Methuen & Co LTD: London, 1969; pp. 235241.

(29) Sajó, I. *Komplexometria*; Műszaki Könyvkiadó Budapest, 1973.

(30) Irving, H. M.; Miles, M. G.; Pettit, L. A study of some problems in determining the stoicheiometric proton dissociation constants of complexes by potentiometric titrations using a glass electrode. *Anal. Chim. Acta* **1967**, *38*, 475−488.

(31) Zékány, L.; Nagypál, I. A Comprehensive Program for the Evaluation of Potentiometric and/or Spectrophotometric Equilibrium Data Using Analytical Derivatives. In *Computational Method for*

Determination of Formation Constants; Springer: New York, 1985. pp 291353.
(32) Evans, D. F. The determination of the paramagnetic susceptibility of substances in solution by nuclear magnetic resonance. *J. Chem. Soc.* **1959**, 2003−2005.
(33) Delgado, R.; Do Carmo Figueira, M.; Quintino, S. Redox method for the determination of stability constants of some trivalent metal complexes. *Talanta* **1997**, *45*, 451−462.
(34) Brausam, A.; Maigut, J.; Meier, R.; Szilágyi, P. A.; Buschmann, H.-J.; Massa, W.; Homonnay, Z.; van Eldik, R. Detailed Spectroscopic, Thermodynamic, and Kinetic Studies on the Protolytic Equilibria of Fe^{III}cydta and the Activation of Hydrogen Peroxide. *Inorg. Chem.* **2009**, *48*, 7864−7884.
(35) Schwarzenbach, G.; Freitag, E. Komplexone XIX. Die Bildungskonstanten von Schwer-metallkomplexen der Nitrilo-triessigsäure. *Helv. Chim. Acta* **1951**, *34*, 1492−1502.
(36) Baranyai, Z.; Pálinkás, Z.; Uggeri, F.; Brücher, E. Equilibrium Studies on the Gd^{3+}, Cu^{2+} and Zn^{2+} Complexes of BOPTA, DTPA and DTPA-BMA Ligands: Kinetics of Metal-Exchange Reactions of $[Gd(BOPTA)]^{2-}$. *Eur. J. Inorg. Chem.* **2010**, *2010*, 1948−1956.
(37) Ma, R.; Motekaitis, R.; Martell, A. Stability of metal ion complexes of *N,N′*-bis (2-hydroxybenzyl) ethylenediamine-N,N′-diacetic acid. *Inorg. Chim. Acta* **1994**, *224*, 151−155.
(38) Giesel, F. L.; von Tengg-Kobligk, H.; Wilkinson, I. D.; Siegler, P.; von der Lieth, C.-W.; Frank, M.; Lodemann, K. P.; Essig, M. Influence of Human Serum Albumin on Longitudinal and Transverse Relaxation Rates (R_1 and R_2) of Magnetic Resonance Contrast Agents. *Invest. Radiol.* **2006**, *41*, 222−228.
(39) Koppenol, W. H. Names for inorganic radicals (IUPAC recommendations 2000. *Pure Appl. Chem.* **2000**, *72*, 437−446.
(40) May, P. M.; Linder, P. W.; Williams, D. R. Computer simulation of metal-ion equilibria in biofluids: models for the low-molecular-weight complex distribution of calcium(II), magnesium-(II), manganese(II), iron(III), copper(II), zinc(II), and lead(II) ions in human blood plasma. *J. Chem. Soc., Dalton Trans.* **1977**, 588−595.
(41) Koppenol, W. H.; Hider, R. H. Iron and redox cycling. Do's and don'ts. *Free Radic. Biol. Med.* **2019**, *133*, 3−10.
(42) Tur'yan, Y.; Kohen, R. Mechanism of Dehydro-L-ascorbic Acid Reduction at Mercury Dropping Electrode. *J. Electroanal. Chem.* **1995**, *380*, 273−290.
(43) Taqui Khan, M. M.; Martell, A. E. The kinetics of the reaction of iron(III) chelates of aminopolycarboxylic acids with ascorbic acid. *J. Am. Chem. Soc.* **1968**, *90* (13), 3386−3389.
(44) Pelizzetti, E.; Mentasti, E.; Pramauro, E. Kinetics and mechanism of the oxidation of ascorbic acid by tris(1,10-phenanthroline)iron(III) and its derivatives in aqueous acidic perchlorate media. *Inorg. Chem.* **1976**, *15* (11), 2898−2900.
(45) Pelizzetti, E.; Mentasti, E.; Pramauro, E. Outer-sphere oxidation of ascorbic acid. *Inorg. Chem.* **1978**, *17* (5), 1181−1186.
(46) Kubíček, V.; Tóth, É. Design and function of metal complexes as contrast agents in MRI. *Adv. Inorg. Chem.* **2009**, *61*, 63−129.
(47) Helm, L.; Morrow, J. R.; Bond, C. J.; Carniato, F.; Botta, M.; Braun, M.; Baranyai, Z.; Pujales-Paradela, R.; Regueiro-Figueroa, M.; Esteban- Gomez, D., et al. *Contrast Agents for MRI: experimental Methods*; The Royal Society of Chemistry: Cambridge, UK, 2018.
(48) Solomon, I. Relaxation Processes in a System of Two Spins. *Phys. Rev.* **1955**, *99*, 559−565.
(49) Bloembergen, N. Proton Relaxation Times in Paramagnetic Solutions. *J. Chem. Phys.* **1957**, *27*, 572−573.
(50) Bloembergen, N.; Morgan, L. O. Proton Relaxation Times in Paramagnetic Solutions. Effects of Electron Spin Relaxation. *J. Chem. Phys.* **1961**, *34*, 842−850.
(51) Koenig, S. H.; Brown, R. D. Field-cycling relaxometry of protein solutions and tissue: Implications for MRI. *Prog. Nucl. Magn. Reson. Spectrosc.* **1990**, *22*, 487−567.
(52) Aime, S.; Botta, B.; Esteban-Gómez, D.; Platas-Iglesias, C. Characterisation of magnetic resonance imaging (MRI) contrast agents using NMR relaxometry. *Mol. Phys.* **2019**, *117*, 898−909.
(53) Swift, T. J.; Connick, R. E. NMR-Relaxation Mechanisms of O^{17} in Aqueous Solutions of Paramagnetic Cations and the Lifetime of Water Molecules in the First Coordination Sphere. *J. Chem. Phys.* **1962**, *37*, 307−320.
(54) Rolla, G. A.; Platas-Iglesias, C.; Botta, M.; Tei, L.; Helm, L. ^1H and ^{17}O NMR Relaxometric and Computational Study on Macrocyclic Mn(II) Complexes. *Inorg. Chem.* **2013**, *52* (6), 3268−3279.
(55) Dumas, S.; Jacques, V.; Sun, W.-C.; Troughton, J. S.; Welch, J. T.; Chasse, J. M.; Schmitt-Willich, H.; Caravan, P. High relaxivity MRI contrast agents part 1: Impact of single donor atom substitution on relaxivity of serum albumin-bound gadolinium complexes. *Invest. Radiol.* **2010**, *45* (10), 600−612.
(56) Jacques, V.; Dumas, S.; Sun, W.-C.; Troughton, J. S.; Greenfield, M. T.; Caravan, P. High relaxivity MRI contrast agents part 2: Optimization of inner- and second-sphere relaxivity. *Invest. Radiol.* **2010**, *45* (10), 613−624.
(57) Aime, S.; Barge, A.; Botta Terreno, E. *in Metal Ions in Biological Systems: The Lanthanides and Their Interrelations with Biosystems*; Sigel, H. eds. CRC Press: 2003; Vol. *40*.
(58) Zhang, Z.; Greenfield, M. T.; Spiller, M.; McMurry, T. J.; Lauffer, R. B.; Caravan, P. Multilocus binding increases the relaxivity of protein-bound MRI contrast agents. *Angew. Chem., Int. Ed.* **2005**, *44* (41), 6766−6769.
(59) Dockal, M.; Carter, D. C.; Rüker, F. Conformational transitions of the three recombinant domains of human serum albumin depending on pH. *J. Biol. Chem.* **2000**, *275*, 3042−3050.
(60) Ferreira, M. F.; Mousavi, B.; Ferreira, P. M.; Martins, C. I. O.; Helm, L.; Martins, J. A.; Geraldes, C. F. G. C. Gold nanoparticles functionalised with stable, fast water exchanging Gd^{3+} chelates as high relaxivity contrast agents for MRI. *Dalton Trans.* **2012**, *41*, 5472−5475.
(61) Dattelbaum, J. D.; Abugo, O. O.; Lakowicz, J. R. Synthesis and characterization of a sulfhydryl-reactive rhenium metal−ligand complex. *Bioconjugate Chem.* **2000**, *11*, 533−536.
(62) Troughton, J. S.; Greenfield, M. T.; Greenwood, J. M.; Dumas, S.; Wiethoff, A. J.; Wang, J.; Spiller, M.; McMurry, T. J.; Caravan, P. Synthesis and evaluation of a high relaxivity manganese (II)-based MRI contrast agent. *Inorg. Chem.* **2004**, *43*, 6313−6323.
(63) Fries, P. H.; Belorizky, E. Electronic relaxation of paramagnetic metal ions and NMR relaxivity in solution: Critical analysis of various approaches and application to a Gd(III)-based contrast agent. *J. Chem. Phys.* **2005**, *123*, 124510−124525.

https://doi.org/10.1021/acs.inorgchem.4c01715
Inorg. Chem. 2024, 63, 12992−13004